Inorganic Chemistry
Article

Inorg. Chem. **2010**, *49*, 249–260 **249**
DOI: 10.1021/ic901936s

Playing the Quantum Chemical Slot Machine: An Exploration of ABX_2 Compounds

Xiao-Dong Wen, Thomas J. Cahill, Nicholas M. Gerovac, Michael J. Bucknum, and Roald Hoffmann*

Department of Chemistry and Chemical Biology, Cornell University, Baker Laboratory, Ithaca, New York 14853-1301

Received October 1, 2009

The structures and electronic properties of a number of real and hypothetical ABX_2 compounds sharing (or evolving from) a single *P*4/*mmm* structural type are examined. These include the known $CaCuO_2$ and $SrFeO_2$ phases. A number of variations of this *P*4/*mmm* ABX_2 framework, some obvious, some exotic, all with a chemical motivation, were investigated: A = alkali metal, alkaline earth metal or La, B = Ti, Fe, Cu, or Pt, and X = C, O, S, C_2, H_2, or F. Careful attention was given to the d-orbital splitting patterns and magnetic states (ferromagnetic or antiferromagnetic) of these compounds, as well as their stability gauged by phonon dispersions and energetics. The most interesting as yet unmade compounds that emerged were (a) a carbide $SrFe(C_2)_2$, containing C_2 units with a C−C distance of 1.267 Å, (b) an $AeTiO_2$ series, with Ti−Ti bonding, part σ, part π, tuned by the Ae^{2+} cation size, and (c) $NaPtF_2$, for which a second structure was found, containing a hexagonal layering of $(PtF_2)^-$ molecules.

1. Introduction

An intriguing 4,6,8-connected tetragonal structure of ABX_2 stoichiometry was suggested by M. J. Bucknum, who termed it "Kentuckia".[1,2] Two views of the structure are shown: Figure 1 (top) is the primitive unit cell, *P*4/*mmm*. Figure 1 (bottom) shows the super cell, ($\sqrt{2} \times \sqrt{2} \times 1$), containing two ABX_2 units. The Wyckoff positions in the primitive unit cell are A (1/2, 1/2, 1/2), B (0, 0, 0), X (0, 1/2, 0), and X (1/2, 0, 0). Note the cubical coordination of atom A, the BX_2 sheets with a square-planar environment around B, and the 4 + 2 quasi-octahedral coordination of X.

The primitive unit cell description in Figure 1 clearly shows the relationship of this structure to the familiar ABX_3 perovskite structure; the faint empty circles indicate where the atoms are missing relative to a true perovskite.

It turns out that a realization of the Kentuckia structure had been known for some time, in $CaCuO_2$. Containing typical two-dimensional CuO_2 layers, this structure has been naturally much studied as it is a superconductor (T_c 40 to 110 K).[3] In the ground state, $CaCuO_2$ is insulating (the experimental band gap is 1.5 eV)[4] and antiferromagnetic (AFM).[5] Given the interesting properties of $CaCuO_2$, other isostructural alkaline copper oxides ($AeCuO_2$ with A = Sr or Ba)[6] have been synthesized and investigated.

Recently, other systems crystallizing in this structural type have garnered attention. In a novel synthesis, $LaNiO_2$ was prepared by controlled H_2 reduction of the perovskite $LaNiO_3$[7,8] and in a similar preparation $SrFeO_2$ was synthesized via the reaction of the perovskite $SrFeO_3$ with CaH_2.[9] $SrFeO_2$ contains planar FeO_2 layers with one Fe atom surrounded by four O atoms. Typically, Fe d^6 is either tetrahedrally or octahedrally coordinated, rarely in a square-planar environment, which is one reason for interest in this structure.

A number of theoretical studies have been published on these ABX_2 structures ($CaCuO_2$,[10−15] $LaNiO_2$,[16] $SrFeO_2$[17,18]) (*P*4/*mmm*, space group), typically employing density functional theory (DFT). These computations focused on the electronic structure and magnetism, thus requiring spin-polarized calculations. A variety of exchange-correlation

*To whom correspondence should be addressed. E-mail: rh34@cornell.edu.

(1) Bucknum, M. J.; Castro, E. A. *Russ. J. Gen. Chem.* **2006**, *76*, 265.
(2) Bucknum, M. J. *Chem. Prepr. Arch.* **2002**, *1*, 181.
(3) Siegrist, T.; Zahurak, S. M.; Murphey, D. W.; Roth, R. S. *Nature* **1988**, *334*, 231.
(4) Tokura, Y.; Taguchi, Y.; Okada, Y.; Fujishima, Y.; Arima, T. *Phys. Rev. B* **1990**, *41*, 11 657.
(5) Vaknin, D.; Caignol, E.; Davies, P. K.; Fischer, J. E.; Johnston, D. C.; Goshorn, D. P. *Phys. Rev. B* **1989**, *39*, 9122.
(6) Takano, M.; Takeda, Y.; Okada, H.; Miyamoto, M.; Kusaka, T *Phys. C* (*Amsterdam, Neth.*) **1989**, *159*, 375.
(7) Crespin, M.; Levitz, P.; Gatineau, L. *J. Chem. Soc., Faraday Trans.* **1983**, *79*, 1181.
(8) Crespin, M.; Isnard, O.; Dubois, F.; Choisnet, J.; Odier, P. *J. Solid State Chem.* **2005**, *178*, 1326.
(9) Tsujimoto, Y.; Tassel, C.; Hayashi, N.; Watanabe, T.; Kageyama, H.; Yoshimura, K.; Takano, M.; Ceretti, M.; Ritter, C.; Paulus, W. *Nature* **2007**, *450*, 1062.
(10) Wu, H.; Zheng, Q.; Gong, X.; Lin, H. Q. *J. Phys.: Condens. Matter* **1999**, *11*, 4637.
(11) Wu, H.; Zheng, Q. *J. Phys.: Condens. Matter* **2000**, *12*, 5813.
(12) Rosner, H.; Diviš, M.; Koepernik, K.; Drechsler, S.-L.; Eschrig, H. *J. Phys.: Condens. Matter* **2000**, *12*, 5809.
(13) Fijalkowski, K.; Grochala, W. *Dalton Trans.* **2008**, *40*, 5447.
(14) De La Mora, P.; Tavizón, G. *Int. J. Quantum Chem.* **2000**, *80*, 499.
(15) Feng, X.-B.; Harrison, N. M. *Phys. Rev. B* **2004**, *69*, 132502.
(16) Lee, K.-W.; Pickett, W. E. *Phys. Rev. B* **2004**, *70*, 165109.
(17) Xiang, H. J.; Wei, S.-H. *Phys. Rev. Lett.* **2008**, *100*, 167207.
(18) Pruneda, J. M.; Íñiguez, J.; Canadell, E.; Kageyama, H.; Takano, M. *Phys. Rev. B* **2008**, *78*, 115101.

Published on Web 12/04/2009

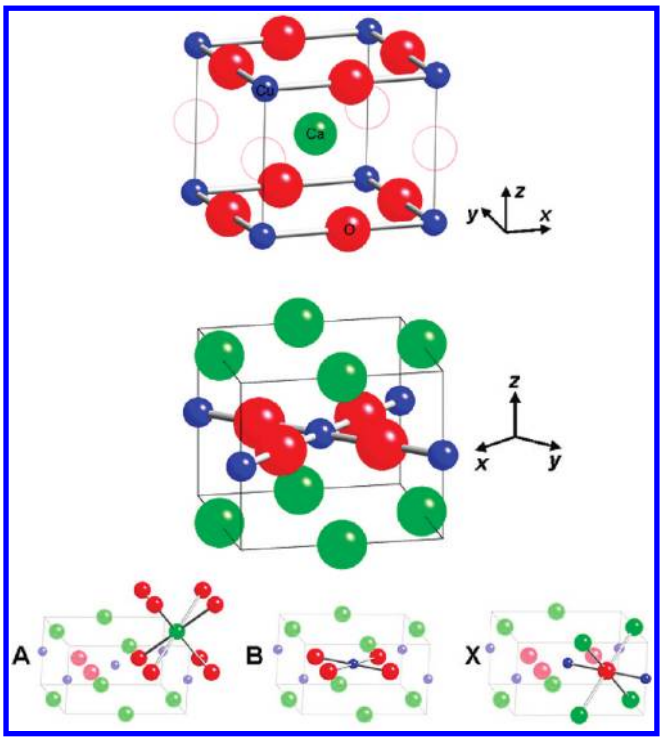

Figure 1. (top) ABX_2 structure, atoms specified for $CaCuO_2$. The relationship to the perovskite structure is emphasized in this view, a true perovskite structure would also include the red atoms indicated by the faint empty circles. (bottom) The ($\sqrt{2} \times \sqrt{2} \times 1$) supercell of an ABX_2 structure. The coordination environment of the individual atoms is emphasized here, square planar for A (green atoms), cubic for B (blue atoms), and approximately octahedral for X (red atoms).

energy functionals, such as LDA, GGA, DFT+U, and so forth have been applied in the calculations. As a result of the strongly correlated nature of transition metals, both the LDA and GGA methods fail to predict the correct magnetic ground state, but often obtain a reasonable approximation of the total density of states (TDOS). We will argue that the magnetism of these systems can be reliably calculated utilizing the local spin density approximation (LSDA) including on-site Coulomb interaction (U) (LSDA+U) method.

In this work we play the molecular slot machine by varying A, B, and X in this ABX_2 system. We do so not at random, but moved by chemical considerations. Careful attention is paid to the magnetic properties (ferromagnetic and antiferromagnetic) for all structures. We consider many different variations for A, B, and X in this framework; the most interesting, for a variety of reasons which will become clear later on, are $CaCuO_2$, $SrFeO_2$, $SrTiO_2$, $SrFeC_2$, $SrFe(C_2)_2$, $SrFe(H_2)_2$, and $NaPtF_2$. The first two exist; the other five are hypothetical compounds and potential synthetic targets. The calculated observables for all structures (lattice parameters, bond distance, magnetic moment, and electronic energy) are listed in the Supporting Information. Phonon dispersion is utilized to probe the dynamic stability of these compounds.

Let us begin with the known systems.

2. Predicting the Structural and Electronic Properties of ABX_2 Compounds

$CaCuO_2$. The environment of Cu in $CaCuO_2$ is square-planar. One expects a classical crystal field splitting for the d-block of four below one, the destabilized orbital being $d_{x^2-y^2}$ (in the coordinate system defined in Figure 1). π-bonding may, and does, split the d_{xz}, d_{yz}, d_{xy} block. The splitting pattern is confirmed by calculations on a molecular CuH_4^{2-} model (Supporting Information).

π-bonding between Cu d and O p orbitals would be expected to perturb this level pattern. The d_{xy} orbital has greater possibilities for d-p π overlap, and should be pushed up relative to $d_{xz} + d_{yz}$. We probed this with a $[Cu(OH)_4]^{2-}$ model and confirmed the effect (see Supporting Information). This model molecule proved to have its own complications, namely, holes in the oxygen p orbitals.

Let us see if these simple orbital ordering ideas are followed in the $CaCuO_2$ electronic structure. This is easiest to do in a spin-unpolarized system, so we first looked at the primitive cell of the spin-unpolarized $CaCuO_2$. For $CaCuO_2$, the calculated parameters (lattice constants a = 3.842 Å, c = 3.195 Å) agree with experiment[19] (a = 3.856 Å, c = 3.181 Å).

The band structure and the different contributions to the density of states (DOS) are shown in Figure 2. Between −6 and 3 eV, there are 10 filled bands, and 1 partially filled band at the Fermi level; these bands are due to the mixing of six O 2p orbitals with five Cu 3d orbitals. Above 3 eV, the unfilled bands can be assigned to Ca 4d orbitals. While the Vienna Ab-initio Simulation Package (VASP) orbital partitioning is unreliable (especially above the Fermi level), it is clear that, as expected, the partially filled band arises from the interaction between O 2p and Cu $3d_{x^2-y^2}$.

Let us take a closer look at the partially filled band in $CaCuO_2$. The orbitals contributing to the band crossed by the Fermi level are shown in Figure 2 at different special k-points in the Brillouin zone. The reason why the partially filled band in Figure 2 is at its highest energy at M is that the Cu $3d_{x^2-y^2}$ − O 2p antibonding interaction is minimized at Γ, maximal at M. The lesser, symmetry-allowed mixing of O 2s into the Γ and X orbitals is not shown here.

Returning to the basic orbital pattern seen in $CaCuO_2$, we focus on the individual d orbital contributions in Figure 2 bottom. The d_{xy} and $d_{x^2-y^2}$ bands appear in a two-peak pattern. It must be that they both interact with oxygen orbitals strongly, the aforementioned π-antibonding for d_{xy}, and σ interactions (as shown in Figure 3) for $d_{x^2-y^2}$. The higher-lying Cu $d_{x^2-y^2}$ − O 2p antibonding band gives rise to the states directly around the Fermi level.

To distinguish AFM and FM structures it is necessary to look at $CaCuO_2$ in a larger supercell, containing at least 4 $CaCuO_2$ units. In this model, the AFM structure is more stable than the FM structure by 0.18 eV per $CaCuO_2$. For AFM $(CaCuO_2)_4$ the calculated structure (lattice constants a = 3.848 Å, c = 3.192, magnetic moment μ = 0.29 μ_B) agrees pretty well with experiment[19] (a = 3.856 Å, c = 3.181 Å, magnetic moment μ = 0.51 μ_B). The calculated phonon dispersion of AFM $CaCuO_2$ shows no imaginary frequency modes, indicating the stability for the phase.

The supercell contains four formula units; thus the band structure will be 4-fold folded back, necessarily

(19) Karpinski, J.; Schwer, H.; Mangelschots, I.; Conder, K.; Morawski, A.; Lada, T.; Paszewin, A. *Phys. C* **1994**, *234*, 10.

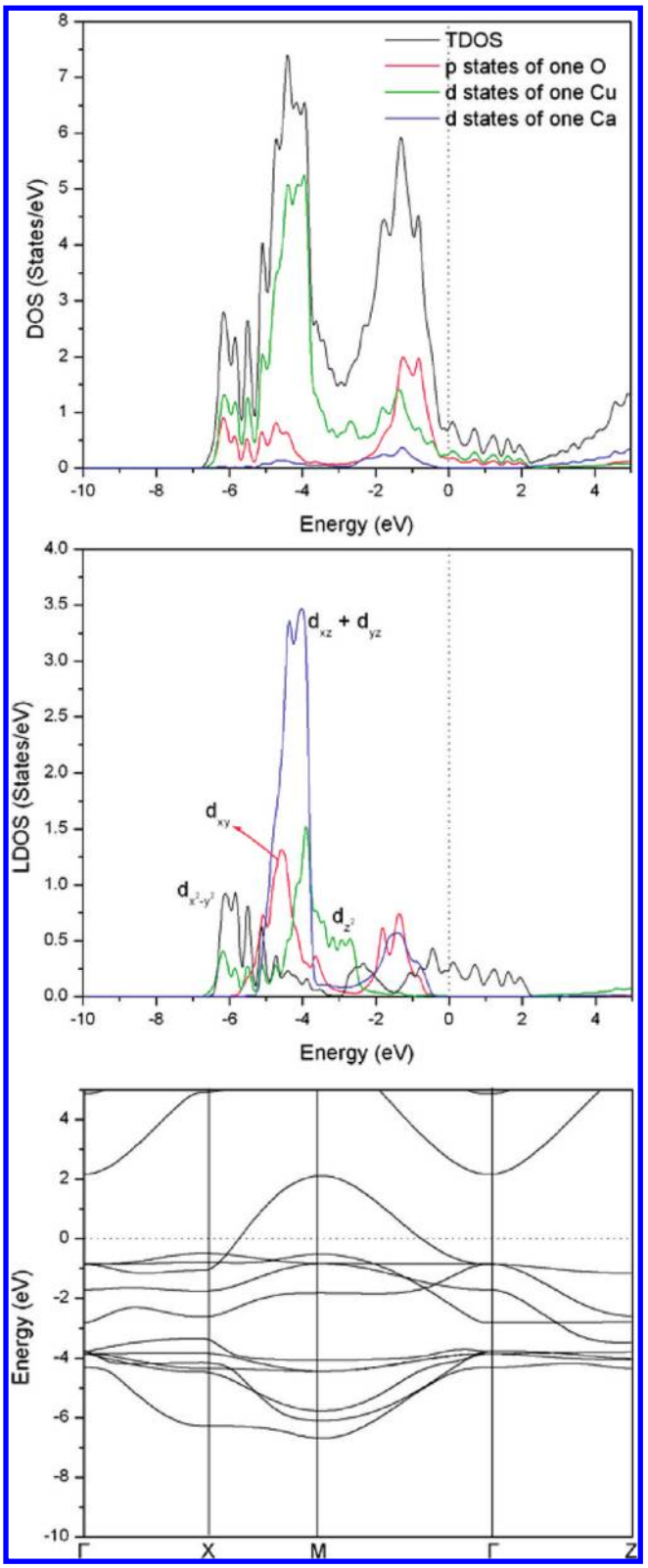

Figure 2. Calculated DOS [The DOS in the region 0 → 2 eV looks undulating, but this is an artifact of the calculation. As the band structure shows there is only one smooth band in this region. A calculation with more *k* points did not improve the appearance of the DOS.] of the spin-unpolarized primitive $CaCuO_2$ structure (DFT). The projected (PDOS) of one O, Cu, and Ca atom are shown. The local density of states (LDOS) of the Cu d orbitals is shown. The dotted line indicates the adjusted Fermi level placed at 0 eV.

appearing more complex than for the spin-unpolarized system (see Supporting Information). Looking at the

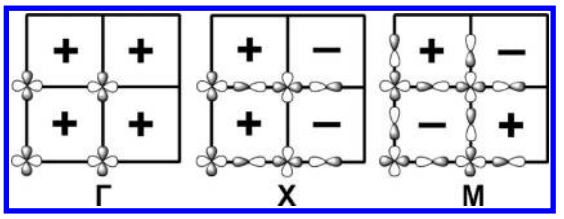

Figure 3. Makeup of the band crossing the Fermi level in $CaCuO_2$, emphasizing the antibonding interaction between Cu $3d_{x^2-y^2}$ and O 2p orbitals at various special *k*-points. Only the square planar Cu−O sublattice is shown. The + and − signs illustrate the phase of the unit cell. The antibonding d-p σ interaction is maximized at M, and minimized at Γ. This explains the dispersion seen in the half-filled band in Figure 2.

individual orbital contributions to the DOS (Figure 4), we see an expected distinction between spin states. To help distinguish between different spin-states (an arbitrary human assignment) we refer to the up or majority spin and down or minority spin. Most of the spin-unpolarized crystal field picture is retained: spin up and down d_{z^2}, $d_{xz} + d_{yz}$, and d_{xy} bands are occupied. In the AFM supercell, we find that the Cu $d_{x^2-y^2}$ is responsible for the Cu contribution at the Fermi level.

Note that the spin polarization is nicely confined to the Cu states. The structural parameters and the Cu d orbital splitting ($z^2 \sim xz$, $yz < xy < x^2-y^2$) of $CaCuO_2$ does not change noticeably from the spin-unpolarized primitive cell to the AFM supercell.

Our computations indicate that $CaCuO_2$ should be metallic, even if it has a low DOS at the Fermi level. This is not correct; experimentally it is known that $CaCuO_2$ is a semiconductor or insulator, with a 1.5 eV band gap.[5] As mentioned earlier, previous theoretical work on $CaCuO_2$ suggests that the LSDA fails to predict correct ground states because of the self-interaction item.[20] In our case, the LSDA+U exchange-correlation functional does locate the correct ground state (AFM) for $CaCuO_2$, but fails to provide us with the known insulating experimental electronic structure. Other calculations[10,15] employing non-plane-wave pseudopotentials, predict $CaCuO_2$ to be an insulator; still these calculations vary in both their band gap and the magnetic moment on Cu.

We tried to induce a band gap in our calculations by varying the Hubbard U and J terms, but these strategies do not work. We continue to look into this computational problem; while the failure to calculate $CaCuO_2$ as insulating is troubling, the DFT results seem reasonable for many of the other compounds we have explored.

$SrFeO_2$. Recently, an FeO_2 square planar layer was reported in the remarkable (because of its relationship to a perovskite) ternary $SrFeO_2$. Fe(II) in $SrFeO_2$ has three less valence electrons than Cu(II) in $CaCuO_2$. With six valence electrons on the metal one could imagine both high-spin and low-spin states for the system.

Our spin-polarized calculations for $SrFeO_2$ (four formula units per unit cell) indicate an AFM structure (0.11 eV per $SrFeO_2$ more favorable than the FM structure). The computed unit cell parameters in the AFM structure (lattice constants a = 4.045 Å, c = 3.484 Å) agree well with experiment (a = 3.985 Å, c = 3.458 Å).[9] The optimized Fe−O bond length is 2.022 Å, corresponding

(20) Pichett, W. E. *Rev. Mod. Phys.* **1989**, *61*, 433.

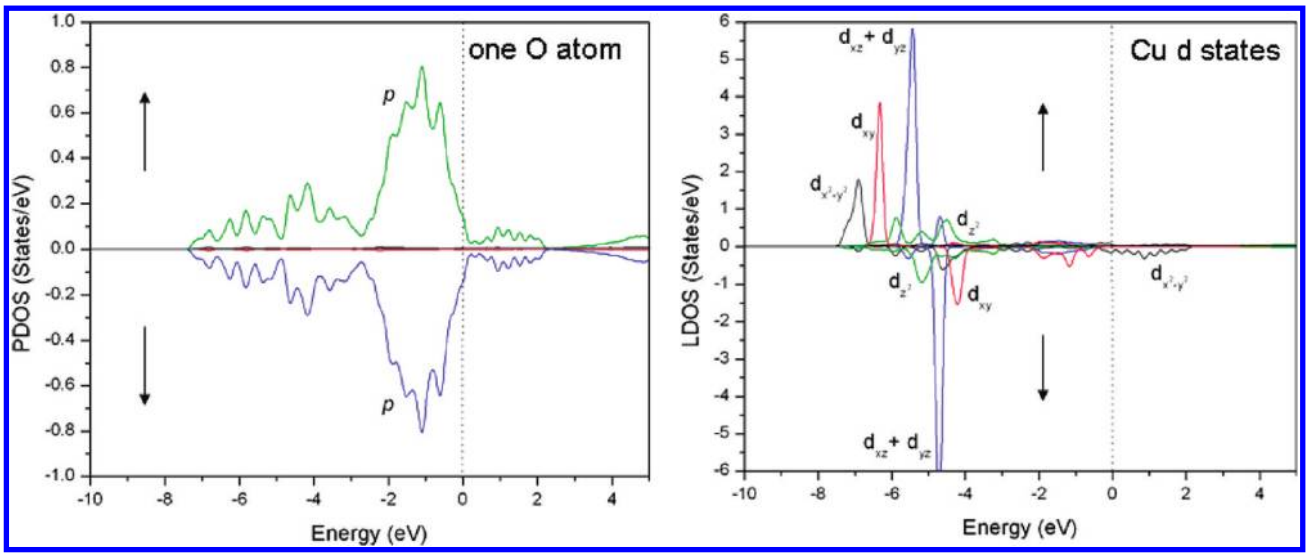

Figure 4. Calculated projected density of states (PDOS) of one O and local density of states (LDOS) of the Cu d orbitals in AFM $CaCuO_2$ supercell structure. The dotted line indicates the adjusted Fermi level placed at 0 eV.

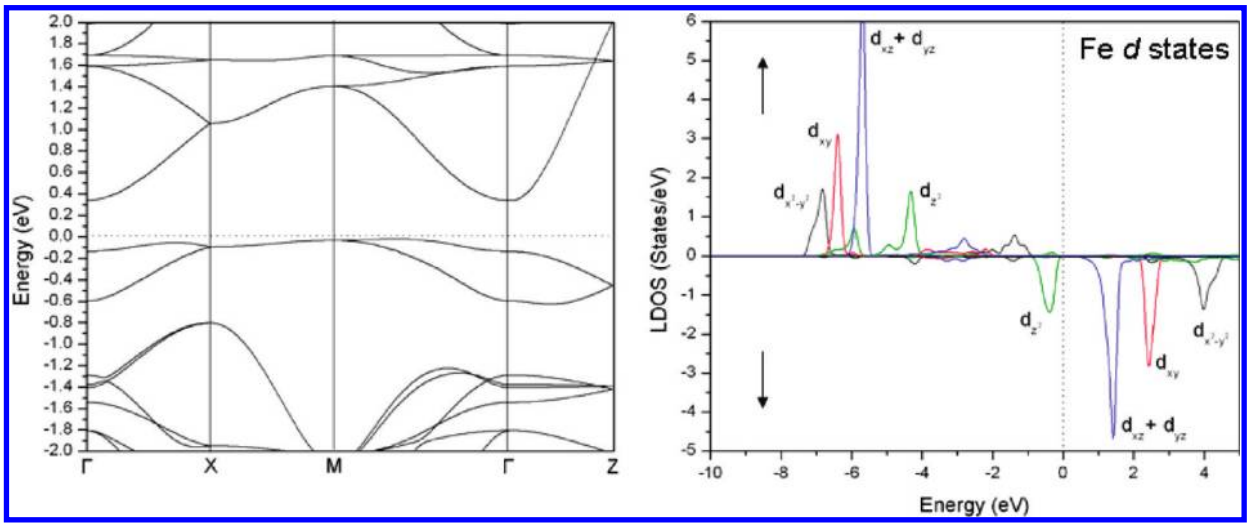

Figure 5. Band structure, local density of states (LDOS) of the Fe d orbitals in AFM $SrFeO_2$. The dotted line indicates the Fermi level.

well to a variety of experimental Fe(II)−O distances: in an octahedral coordination (α-FeO), 2.171 Å;[21] a distorted octahedron (α-Fe_2O_3), 1.946 Å to 2.116 Å;[22] and in Fe_3O_4 (tetrahedral and octahedral coordination), 1.886−2.060 Å.[23] The calculated phonon dispersion shows no imaginary frequency modes.

The band structure and the different contributions to the DOS are shown in Figure 5. We can see from the computed band structure that $SrFeO_2$ is a direct gap semiconductor (the smallest gap located at Γ). No physical measurements of the electronic properties of this phase appear have been published. The oxygen p states approach but do not cross the Fermi level. Each Fe 3d orbital is filled in the majority spin; the minority spin has only the $3d_{z^2}$ filled. Clearly, the computed $SrFeO_2$ structure is high spin with four unpaired electrons, in agreement with experiment.[9] Our computed magnetic moment is 3.7 μ_B, corresponding well to the experimental data[9] (3.6 μ_B at 10 K) and theoretical work.[17,18] Essentially none of the spin polarization is felt by the oxides (see Supporting Information).

The large splitting of spin states for this magnetic metal center makes it difficult to assign a single level ordering diagram that would be appropriate for both spins. For instance, look at the contribution of $d_{x^2-y^2}$ orbitals, they are at low energy for the majority spin, at high energy for the minority spin. Clearly all five d orbitals are occupied for the majority spin. The d_{z^2} orbital is the only one significantly occupied for the minority spin, but at relatively high energy for the majority spin.

The original experimental work on $SrFeO_2$ assigned (apparently based solely on crystal field expectations) three electrons into the $d_{xz} + d_{yz}$ set, as shown in Figure 6b. Subsequent theoretical work[17,18] revised this assignment to have the d_{z^2} orbital doubly occupied, which is what we obtain in our calculation (Figure 6c). Very recently Kawakami et al. found a remarkable

(21) Jette, E. R.; Foote, F. *J. Chem. Phys.* **1933**, *1*, 29.
(22) Blake, R. L.; Hessevick, R. E.; Zoltai, T.; Finger, L. W. *Am. Mineral.* **1966**, *51*, 123.
(23) Wechsler, B. A.; Lindsley, D. H.; Prewitt, C. T. *Am. Mineral.* **1984**, *69*, 754.

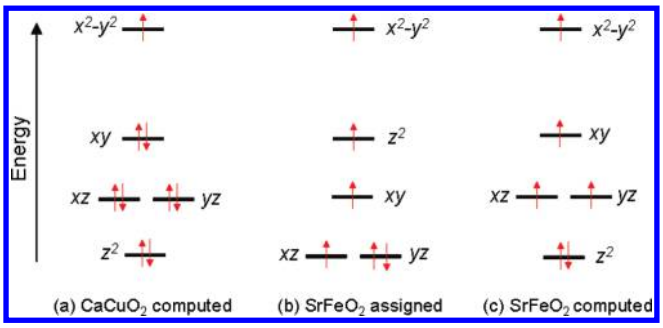

Figure 6. (a) Computed (DFT) d-orbital splitting in $CaCuO_2$; (b) assigned d orbital splitting in $SrFeO_2$; and (c) computed (DFT) d orbital splitting in $SrFeO_2$. The level ordering drawings are schematic; the difficulty of coming to a certain level ordering is discussed in the text.

pressure-induced spin transition in $SrFeO_2$ from an antiferromagnetically coupled insulator to a ferromagnetic half-metallic state. We have not studied the latter state; for the former the spin densities reported are qualitatively similar to those we obtain.[24]

The computed AFM $CaCuO_2$ d level splitting diagram $z^2 \sim xz + yz < xy < x^2 - y^2$ (Figure 6a, with the x,y axes along the M−O bonds) was discussed earlier; it has the same ordering as $SrFeO_2$, but with three additional electrons. It needs to be said again that a single level splitting diagram combining majority and minority spins in one diagram for a highly magnetic material is a gross simplification: a comparison of the schematic of Figure 6 with the calculations of Figure 4 and 5 makes this clear. A similar d splitting diagram (Figure 6b and c) was also discussed by Köhler.[25]

Sulfur is in the same group as oxygen, so we explored $SrFeS_2$. The calculated $SrFeS_2$ AFM structure (lattice constants a = 4.853 Å, c = 3.947 Å) is 0.11 eV more favorable than the FM state. The replacement of O with the larger S caused the unit cell to expand in a and c, as expected (computed $SrFeO_2$ lattice constants a = 4.045 Å, c = 3.484 Å). The computed TDOS (see Supporting Information) indicates that $SrFeS_2$ should be a semiconductor with a small gap, quite similar to $SrFeO_2$. However, the calculated phonon dispersion for $SrFeO_2$ gave imaginary frequency modes at Γ ($\sim 25i$ cm^{-1}), indicative of possible structural instability ($SrFeF_2$ was also optimized and gave large imaginary frequencies). We did not search for a more stable structure. Note that only one ternary Sr−Fe−S compound is known.[26]

$SrFeC_2$. $SrFeC_2$, a hypothetical phase, was formed by substituting C^{4-} for O^{2-}. There are no reported ternary crystal structures of this elemental composition. Nor did we expect this structure to be viable; in it Fe would formally be Fe^{6+}, not a typical oxidation state for the element. Still, out of curiosity, $SrFeC_2$ was optimized in the Kentuckia framework. To our surprise, the calculated phonon dispersion shows no imaginary frequency modes, indicating at least metastability for the phase.

Our spin-polarized calculations for $SrFeC_2$ (four formula units per unit cell) point to an AFM structure (0.65 eV per $SrFeC_2$ more favorable than the FM structure). The computed $SrFeC_2$ unit cell parameters (lattice constants a = 3.777 Å, c = 4.300 Å, $\mu = 2.40\ \mu_B$) are very different than those calculated for $SrFeO_2$. The Fe−C distance is 1.888 Å, which falls within the expected range of Fe−C distances for many structures (see Supporting Information) in the Inorganic Crystal Structure Database (ICSD).

The C and Fe contributions to the DOS of $SrFeC_2$ are shown in Figure 7. We can see that $SrFeC_2$ is metallic. The magnetic moment calculated for Fe in $SrFeC_2$ (μ = 2.40 μ_B) corresponds to roughly three unpaired electrons. Each Fe 3d orbital is filled in the majority spin; the minority spin has only the $3d_{z^2}$ completely filled (the $d_{xz} + d_{yz}$ are half-filled). Clearly, the oxidation state of Fe in the hypothetical $SrFeC_2$ is not +6, but closer to +2. There must be some carbon states unfilled because of electron transfer, and Figure 7 shows a good number of carbon states above the Fermi level.

Interestingly, a series of ABC_2 compounds exists, with a very different structure. In these, $ScT_{1-x}C_2$ (T = Fe, Co, Ni, $x \sim 0.15$), there are C_2 pairs with a C−C distance 1.35−1.40 Å.[27] We thank a reviewer for bringing this structure to our attention.

$SrFe(C_2)_2$. A well-known (and industrially important) compound is CaC_2, which contains Ca^{2+} and C_2^{2-} acetylide units. This led us to think of substituting C_2^{2-} units for O^{2-} in $SrFeO_2$.

Transition metal carbides contain C_2^{2-} units in a variety of orientations.[28] We optimized three different "isomers" (Figure 8). The first isomer (Figure 8a) has the C_2^{2-} units aligned along Fe···Fe, that is, ···Fe··· CC···Fe···. It also made sense also to try structures such as those shown in Figures 8b and 8c, differing from the first isomer by rotation of C_2^{2-} units. The structure shown in Figure 8b has an interesting feature, ···CC··· CC···CC··· needles running through the structure, and π-coordination of C_2^{2-} units to the irons. This π-coordination is also seen in the isomer of Figure 8c, as well as a potentially short C−C contact in the faces.

The FM state was favored in all three by ~0.11 eV per $SrFe(C_2)_2$ unit. The most stable (~1.3 eV per $SrFe(C_2)_2$ relative to the other structures) computed isomeric arrangement is shown in Figure 8a. The calculated unit cell parameters of FM $SrFe(C_2)_2$ are a = 5.058 Å and c = 3.645 Å; this yields a C−C distance of 1.267 Å and an Fe−C distance of 1.896 Å.

Can we understand the computed C−C distance in $SrFe(C_2)_2$, 1.267 Å, which is somewhere between acetylene, 1.20 Å, and ethene, 1.34 Å? Let us build up from a single C_2^{2-} molecule to the carbon sublattice of $SrFe(C_2)_2$. Figure 9 shows a schematic molecular orbital diagram for a C_2^{2-} molecule. The orbitals are familiar! For 10 valence electrons, C_2^{2-}, we note that the highest occupied molecular orbital (HOMO) is a nonbonding lone pair combination, $3\sigma_g$, and the lowest unoccupied molecular orbital (LUMO) is an antibonding orbital, $1\pi_g^*$.

(24) (a) Kawakami, T.; et al. *Nat. Chem.* **2009**, *1*, 371. (b) Whangbo, M.-H.; Köhler, J. *Nat. Chem.* **2009**, *1*, 351.
(25) Köhler, J. *Angew. Chem., Int. Ed.* **2008**, *47*, 4470.
(26) Cenzual, K.; Gelato, L. M.; Penzo, M.; Parthe, E. *Acta Crystallogr., Sect. B* **1991**, *47*, 433.
(27) Pottgen, R.; Jeitschko, W.; Wortmann, U.; Danebrock, M. E. *J. Mater. Chem.* **1992**, *2*, 633.
(28) Jeitschko, W.; Gerss, M. H.; Hoffmann, R.-D.; Lee, S. *J. Less Common Met.* **1989**, *156*, 397.

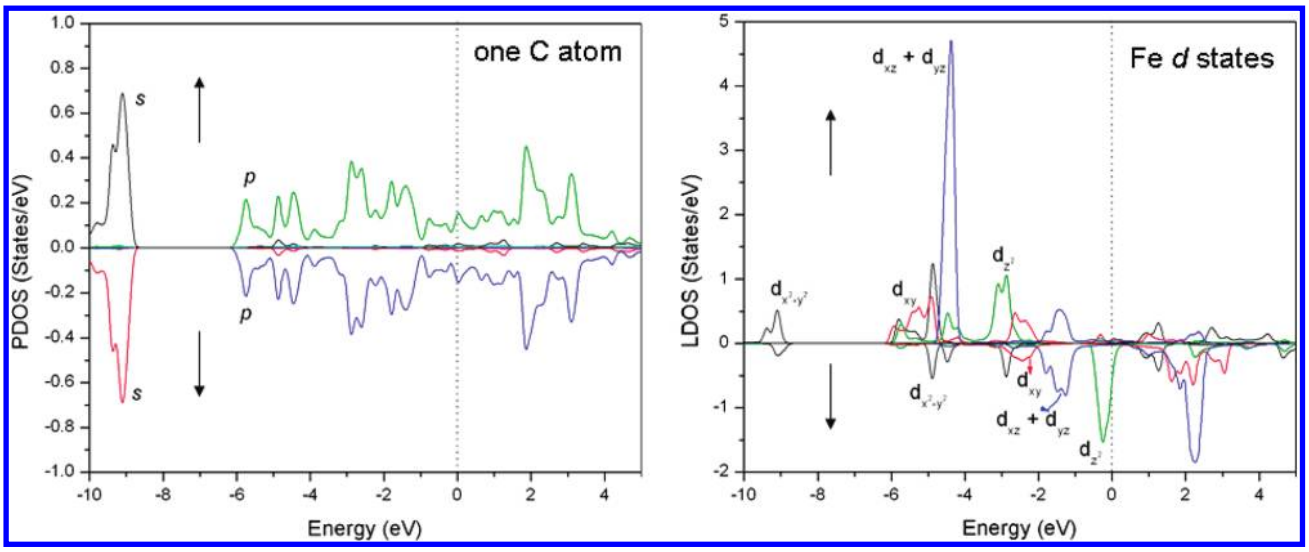

Figure 7. Partial density of states of one C atom and local density of states (LDOS) of the Fe d orbitals in AFM $SrFeC_2$. The dotted line indicates the Fermi level.

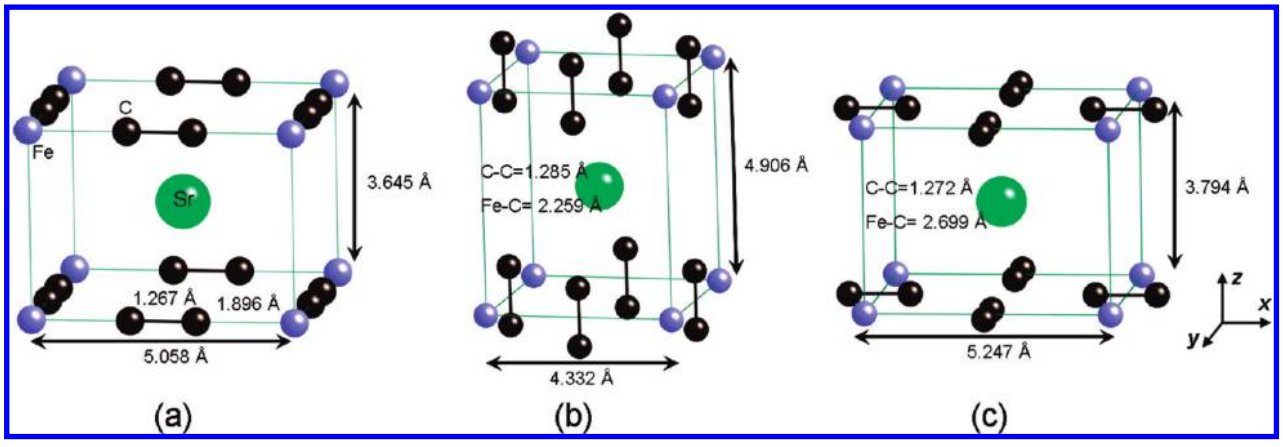

Figure 8. Optimized FM $SrFe(C_2)_2$ isomeric structures (DFT).

To help assign the orbital ordering in the extended material, single point DFT calculations of the C_2^{2-} molecule, maintaining the 1.267 Å C−C distances, were performed in a large unit cell (C_2^{2-} units separated by 10 Å) to avoid potential interactions between neighboring carbons. The band structure and DOS are shown in the Supporting Information. From this, we went to the C_2^{2-} sublattice isolated of the $SrFe(C_2)^{2-}$ structure. In Figure 10, the DOS regions are labeled by their isolated molecular levels origin. The unit cell contains two C_2^{2-} molecules, which interact somewhat through space. As one would anticipate from the geometry of the structure (Figure 8) and the makeup of the C_2^{2-} orbitals (Figure 9), the $2\sigma_u$* and $3\sigma_g$ bands, made up from lone pairs pointing out from each molecule, are the ones most dispersed. Even at this stage we see that the bands arising from $3\sigma_g$ and $1\pi_g$* are just touching, so that $1\pi_g$* will begin to be occupied in the sublattice. The additional interactions due to mixing of C_2^{2-} states with Fe d orbitals in $SrFe(C_2)_2$ must push some antibonding $1\pi_g$* states below the Fermi level. The net outcome is a C−C bond that is slightly longer than a typical triple bond.

The C−C separation in carbides ranges from 1.19 Å (in CaC_2) to 1.48 Å.[28] The simple valence bond description of a range of C_2 reduction from C_2^{2-} (triple bond) to C_2^{6-} (single bond) explains most but not all of this; a more detailed molecular orbital (MO) analysis, some of which we have done in our group,[29−34] is needed. The 1.267 Å C−C distance computed makes sense for small occupation of the molecular $1\pi_g$* levels.

The total density of states (Figure 11) of $SrFe(C_2)_2$ differs from $SrFeO_2$. There is a large gap at the Fermi level in the majority spin, while the minority spin crosses the Fermi level. The material appears to be a half-metal. The computed magnetic moment on Fe is 2.4 μ_B, which is lower than in $SrFeO_2$ (3.7 μ_B) and corresponds roughly to three unpaired electrons (see Supporting Information). The partial density of states reveals that the Fe d ($d_{xz} + d_{yz}$) minority-spin states cover the Fermi level; there is also an interesting small contribution from C.

(29) Li, J.; Hoffmann, R. *Chem. Mater.* **1989**, *1*, 83.
(30) Meyer, H.-J.; Hoffmann, R. *Z. Anorg. Allg. Chem.* **1992**, *607*, 57.
(31) Deng, H.; Hoffmann, R. *Inorg. Chem.* **1993**, *32*, 1991.
(32) Long, J. R.; Meyer, H.-J.; Hoffmann, R. *Inorg. Chem.* **1992**, *31*, 1734.
(33) Long, J. R.; Halet, J.-F.; Saillard, J.-Y.; Hoffmann, R.; Meyer, H.-J. *New J. Chem.* **1992**, *16*, 839.
(34) Merschrod, E. F.; Tang, S. H.; Hoffmann, R. *Z. Naturforsch.* **1998**, *53b*, 322.

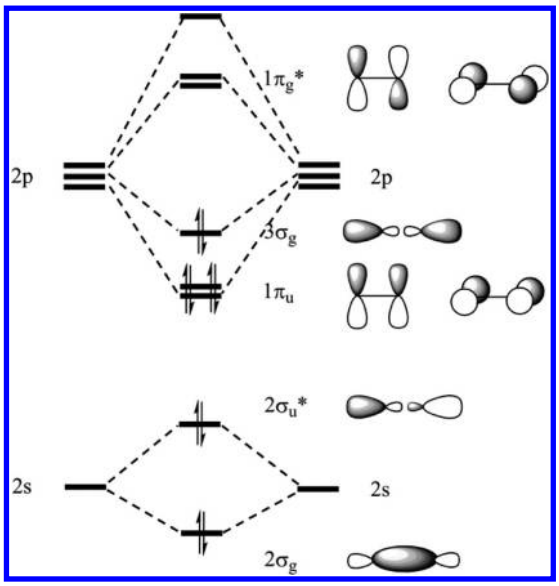

Figure 9. Schematic molecular orbital diagram of C_2^{2-}. The dashed lines indicated the primary parentage of the orbitals; the 2s-2p mixing is included on the orbital representations of the σ_g and σ_u* orbitals.

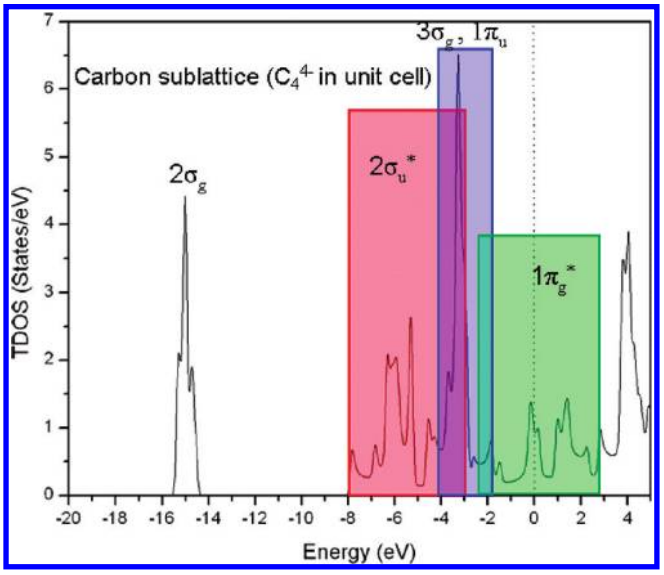

Figure 10. TDOS of the isolated carbon sublattice in $SrFe(C_2)_2$. The dotted line indicates the Fermi level.

In the minority spin states, the d_{xy} is filled, while d_{z^2} is empty. It is not easy to assign the d orbital ordering in $SrFe(C_2)_2$. The spread of the magnetism to the carbide is remarkable; this was not observed in any of the oxides we studied.

Phonon dispersion calculations on $SrFe(C_2)_2$ did not converge. Could there be another more stable geometry with this stoichiometry? To satisfy our curiosity, annealing molecular dynamics (MD) calculations were undertaken on $SrFe(C_2)_2$. The MD calculations revealed a new structure, *Cm* space group, shown in Figure 12, more thermodynamically stable by 0.51 eV than the ABX_2 $SrFe(C_2)_2$ structural type. This geometry may be seen as a shearing deformation of the previous one; the layers have slid relative to each other but the C−C distance (1.26 Å) is maintained. However, the phonon dispersion calculation on this structure did not converge.

An interesting set of recently published compounds is $Sc_3M(C_2)_2$ with M = Fe, Co.[35] In these, C_2 units (C−C = 1.45 Å) bridge square-planar M atoms, in a very different way from the structure shown in Figure 12. The C_2 units are significantly more electron-rich in $Sc_3M(C_2)_2$ than in our stoichiometry. We thank a reviewer for bringing these structures to our attention.

Utilizing the USPEX program, an evolutionary structure prediction, another structure of $SrFeC_4$ (P1) is obtained, still lower in energy. This is shown in Figure 13. The buckled FeC_4 sheets (Figure 13 right) consist of one-dimensional zigzag Fe−Fe chains (Fe−Fe = 2.52/2.50 Å) and dehydropentalene chains (C−C = 1.44−1.50 Å). The structure is more thermodynamically favored by 1.15 eV per $SrFeC_4$ than the Kentuckia $SrFe(C_2)_2$, and more stable by 0.64 eV than *Cm* $SrFeC_4$ obtained by annealing. However, the phonon dispersion calculation on this structure also did not converge. We are not absolutely sure that we have yet found the most stable $SrFe(C_2)_2$ geometry.

$SrFe(H_2)_2$. Straying even further from $SrFe(C_2)_2$, $SrFe(H_2)_2$ was investigated. A quick search of the ICSD revealed no phases known containing only Sr, Fe, and H. If the H_2 units were intact, the oxidation state of Fe would be the unlikely −2 (there in $Fe(CO)_4^{2-}$, but not in extended structures). So reduction of H_2 is likely. We found two structures by optimization from the Kentuckia-like geometries of Figure 8, and a more stable structure by an USPEX search. The two most stable phases are shown in Figure 14.

We focus our discussion on the more thermodynamically stable isomer, $SrFeH_4$ (Figure 14 left). In $SrFeH_4$, the AFM state ($\mu = 3.6\,\mu_B$) is favored over FM by 0.12 eV per formula unit. The structure is unusual, each Fe is involved in eight H bridges to other Fe ions; the Fe−H distance is 2.078 Å, which is within the range of a typical bridging Fe−H bond. Unfortunately, the phonon dispersion calculations on $SrFeH_4$ showed imaginary frequencies.

A dynamically stable structure emerged from the USPEX search, $SrFeH_4$ (USPEX) in Figure 14 right. Each Fe atom is bonded to two top H atoms (Fe−H = 1.77 and 1.92 Å) and four bridge H atoms (Fe−H = 2 × 1.86, 2 × 1.94 Å; Fe−H−Fe = 161°). The environment of an Fe atom in $SrFeH_4$ (USPEX) is approximately octahedral, and the d-electron count is formally 6. The magnetism ($\mu = 2.7\,\mu_B$) indicates that we do not have a simple "t_{2g}" below "e_g" octahedral splitting. Detailed analysis of the band structure (in the Supporting Information) indicates substantial covalence, Fe−H interactions, and an approximate $d_{xz}^2 d_{yz}^2 d_{xy}^1 d_{z^2}^1$ configuration.

$SrTiO_2$. The Kentuckia ABX_2 structure can be thought of as a defect perovskite, as shown in Figure 1. Explaining other realizations of this structural type, we come to $SrTiO_2$, related to the classical $SrTiO_3$ perovskite.

Our spin-polarized calculations [For Ti, U = 4.5 and J = 0. Removing the Hubbard U from the calculation does not change the TDOS or phonon dispersion but decreases the Ti−Ti distance in the *c* direction (3.647 Å→3.589 Å). The different U terms, bond lengths, and DOS are located in the Supporting Information.] for $SrTiO_2$ (four formula

(35) Rohrmoser, B.; et al. *J. Am. Chem. Soc.* **2007**, *129*, 9356.

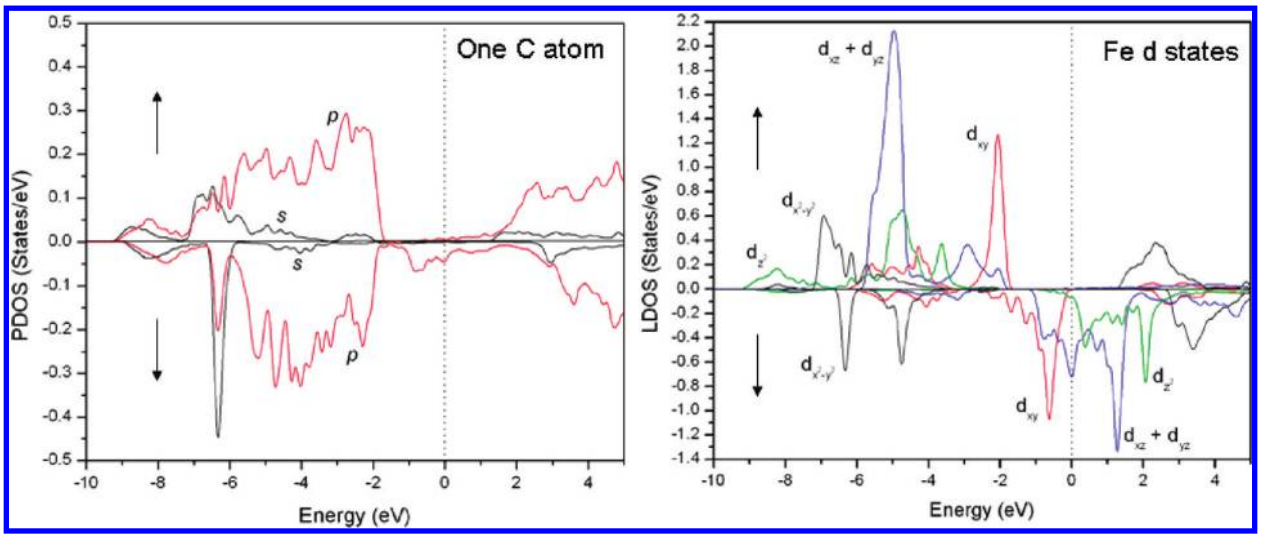

Figure 11. Partial density of states of one C atom and local density of states (LDOS) of the Fe d orbitals in FM $SrFe(C_2)_2$. The dotted line indicates the Fermi level.

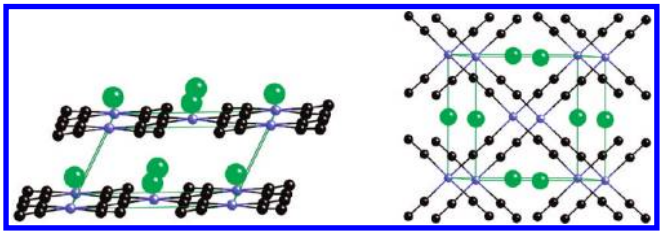

Figure 12. Two views of the optimized FM *Cm* $SrFe(C_2)_2$ structure.

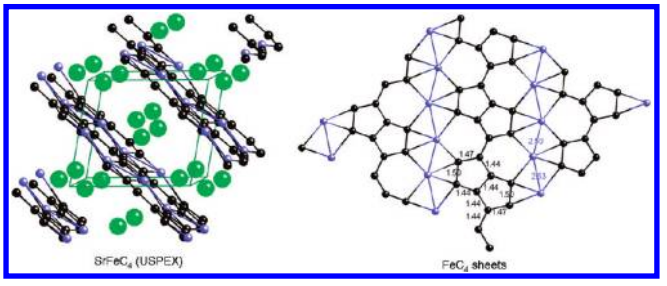

Figure 13. Lowest energy $SrFeC_4$ (P1) structure by USPEX (left), and FeC_4 sheets in it (right).

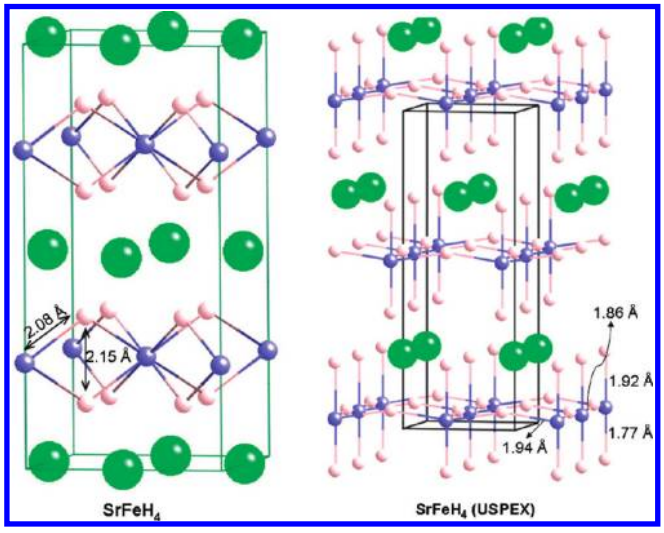

Figure 14. Optimized Kentuckia-like $SrFeH_4$ and lowest energy $SrFeH_4$ (*Amm*2) structure by USPEX.

units per unit cell) indicate a nonmagnetic structure (μ = 0.00 μ_B, AFM and FM calculations identical). The computed $SrTiO_2$ structure (lattice constants a = 4.036 Å, c = 3.647 Å) has a Ti−O distance of 2.018 Å, which falls well within the expected range of Ti−O distance for many structures (see Supporting Information) in the ICSD. Phonon dispersion calculations show no imaginary frequencies.

The band structure of $SrTiO_2$ in a small window around the Fermi level is shown in Figure 15. The band structure immediately jumps out as unusual. The behavior of the levels along the Γ→Z direction is characteristic of a one-dimensional metallic chain.[36,37] This was confirmed by calculation on two simplified one-dimensional models for $AeTiO_2$: naked Ti^{2+} chains; and a $[Ti(OH)_4]^{2-}$ model (Supporting Information). The d_{xy} bands appear to almost touch the Fermi level but not to cross it. Yet, seven valence bands (2 × 3 for the O^{2-} 2p, plus one for the Ti^{2+}) must be occupied, so in some regions of the Brillouin zone states that are not d_{z^2} must be found below the Fermi level. The band structure shows that a degenerate $d_{xz} + d_{yz}$ band crosses the Fermi level, and is partially occupied.

The partially occupied band is made up of $d_{xz} + d_{yz}$, going down in energy from R→Γ. This bonding pattern is present in all the five Kentuckia phases studied.

The computed Ti−Ti distances are long, 3.647 Å, yet the partially occupied d_{z^2} band hints at Ti−Ti bonding, part σ, part π (partial occupation of bonding d_{xz}, d_{yz} states). This led us to further investigation of this system.

If Ti−Ti bonding is present, why do not the layers come closer together upon optimization? We posited that it is the less glamorous (at least in this paper) alkaline earth metals that are responsible for halting the c direction contraction. We substituted Sr in $SrTiO_2$ with two other alkaline earth metals, Ca (smaller radius than Sr) and Ba

(36) Hoffmann, R. *Solids and Surfaces: A Chemist's View of Bonding in Extended Structures*; Wiley-VCH: New York, 1988.
(37) Burdett, J. K. *Chemical Bonding in Solids*; Oxford University Press: Oxford, U.K., 1995

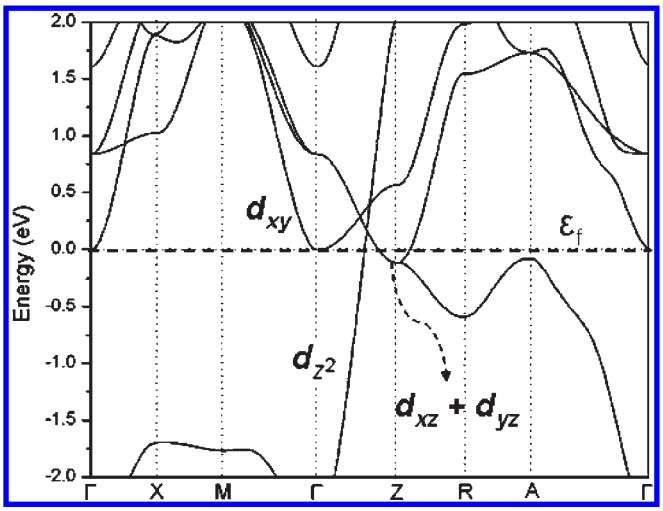

Figure 15. Band structure (red dotted line) of nonmagnetic $SrTiO_2$ around the Fermi level (−2 to 2 eV) for $SrTiO_2$. The dotted line indicates the Fermi level. The corresponding DOS is shown in the Supporting Information.

Table 1. Computed Lattice Constants (DFT), the Ti−Ti OP Values (eH), Magnetic States and Dynamic Stability (Based on Phonon Dispersion) in Five $AeTiO_2$

	a (Å)	*c* (Å) = Ti−Ti	OP of Ti−Ti	magnetic state	dynamically stable
$BeTiO_2$	3.911	2.856	0.36	NM	no
$MgTiO_2$	3.958	3.105	0.35	NM	no
$CaTiO_2$	3.993	3.332	0.34	NM	yes
$SrTiO_2$	4.036	3.647	0.29	NM	yes
$BaTiO_2$	4.075	4.129	0.23	FM	yes

(larger radius than Sr), to look for some sort of size-dependent trend (Table 1). As the ionic radii increase (Ca < Sr < Ba), the *c* direction expands significantly, indicating that the size of the alkaline earth metal plays an important role in determining the Ti−Ti distance. Phonon dispersion calculations of both $CaTiO_2$ and $BaTiO_2$ show no imaginary frequencies.

A still larger series of alkaline earth cations, A = Be, Mg, Ca, and Ba, in ABX_2 provides a consistent picture (Table 1). Clearly, the alkaline earth metal plays a large role in tuning of the electronic properties of the material. The counterion also has an influence on stability: the Be and Mg compounds show imaginary frequencies and so may be unstable in this structure. The other counterions, Ca, Sr, and Ba, all are stable in a phonon study. The related perovskites $BeTiO_3$, $MgTiO_3$, $CaTiO_3$, $SrTiO_3$, and $BaTiO_3$ all exist experimentally. No defect ABX_2 analogues have yet been synthesized of any of these compounds, though we have recently made an attempt.

Note that for all of the compounds, there is Ti−Ti bonding as gauged by the OP values. Remarkably, this bonding is maintained even for quite long Ti−Ti separations. The electronic structure of this group of Ti^{2+}, d^2 compounds, shows metal−metal bonding in a partially ionic structure and that metal−metal bonding is tuned by surrounding cations. The situation is novel, and so we concentrated on providing a firmer basis for the existence

(38) Wen, X.-D.; Cahill, T.; Hoffmann, R.; Miura, A. *J. Am. Chem. Soc.* **2009**, *131*, 14632.

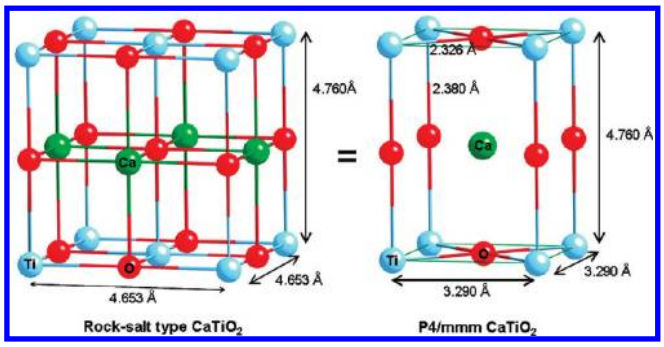

Figure 16. Rock-salt type $CaTiO_2$ structure.

of these phases in a separate paper.[38] Here we just give the highlights of what we found.

First, several obvious reactions of the Kentuckia $AeTiO_2$ compounds were explored; they are decomposition to stable oxides AeO and TiO_2 and "burning" with O_2 to the corresponding perovskites. The first reaction is endothermic, the second exothermic.

We also explored a variety of alternative structures, based on chemical analogy, intuition, and an evolutionary structure searching algorithm. Given that CaO and TiO_2 go into a rock-salt structure, a "rock-salt" geometry (Figure 16) makes sense. Indeed such a structure is more stable than Kentuckia for Ae = Be, Mg, and Ca. Still other less ordered variants (more details in the Supporting Information) of the rock salt motif come out of the evolutionary searching algorithm.

Kentuckia or rock-salt, the $AeTiO_2$ series is a fascinating group of structures with tunable Ti−Ti bonding.

$NaPtF_2$. Straying even further from $CaCuO_2$ or $SrFeO_2$, we looked at $APtF_2$, A = Li, Na, K, and Cs. There are no reported compounds that combine these three elements, and the Pt oxidation state (formally +1) is unusual, which is one reason for our interest in this structure. Square planar coordination is typical of Pt(II), and so is stacking with Pt···Pt interactions, both in this oxidation state and in doped and oxidized compounds of the platinum blue type. The Kentuckia geometry offers the potential for realizing Pt−Pt bonding in an extended structure.

For $NaPtF_2$, the calculated AFM [For Pt, $U = 7.5$ and $J = 0$.] state (lattice constants $a = 4.426$ Å, $c = 3.042$ Å) is favored over the FM state by 0.05 eV per $NaPtF_2$. The Pt−F distance (2.213 Å) is longer than the average length (1.90 Å) observed in known solid state compounds (PtF_4, PtF_5, and PtF_6)[39] and the sum of the atomic covalent radii[40] (1.93 Å). The Pt−Pt separation along the *c* direction is 3.042 Å; longer than the 2.807 Å Pt−Pt distance in the bulk (fcc)[41] metal. This Pt−Pt distance is comparable with Pt−Pt separations between square planar platinums in the platinum blues (2.779−2.885 Å);[42] in these compounds the oxidation state of Pt is fractionally greater than +2.

Compared with the optimized $CaCuO_2$ structure, $NaPtF_2$ appears "flattened" along the *c* direction; the

(39) (a) Mueller, B. G.; Serafin, M. *Eur. J. Solid State Inorg. Chem.* **1992**, *29*, 625. (b) Marx, R.; Seppelt, K.; Ibberson, R. M. *J. Chem. Phys.* **1996**, *104*, 7658.

(40) Cordero, B.; Gómez, V.; Platero-Prats, A. E.; Revés, M.; Echeverría, J.; Cremades, E.; Barragán, F.; Alvarez, S. *Dalton Trans.* **2008**, *21*, 2832.

(41) Davey, W. P. *Phys. Rev.* **1925**, *25*, 753.

(42) Barton, J. K.; Best, S. A.; Lippard, S. J.; Walton, R. A. *J. Am. Chem. Soc.* **1978**, *100*, 3785.

Table 2. Computed Lattice Constants (DFT), the Pt−Pt OP Values (eH),), Magnetic States and Dynamic Stability (Based on Phonon Dispersion) in Four $APtO_2$ Compounds

	a (Å)	c (Å) = Pt−Pt	OP of Pt−Pt	magnetic state	dynamically stable
$LiPtF_2$	4.392	2.869	0.09	AFM	no
$NaPtF_2$	4.426	3.042	0.05	AFM	no
$KPtF_2$	4.503	3.543	0.01	AFM	yes
$CsPtF_2$	4.554	4.074	0.00	AFM	no

a/c ratio is 1.46, larger than 1.21 in $CaCuO_2$. This may also be an indication of some Pt−Pt bonding along the c direction. The total OP value for the Pt−Pt interaction in the c direction is 0.05, a small net bonding effect. We also studied AFM $LiPtF_2$, $KPtF_2$, and $CsPtF_2$ (for the three structures, AFM is more favorable than FM) and found a general trend in Pt−Pt distance at the alkali metal was changed (Table 2). Like $AeTiO_2$, in the $APtF_2$, the spatial requirements of the largest cations (here Cs^+) break the weak Pt−Pt bond, moving the layers further apart. In phonon calculations, the Li and Cs compounds show imaginary frequencies, while the K variant is dynamically stable.

The band structure indicates that $NaPtF_2$ is semimetallic, with a tiny band gap, as shown in Supporting Information. The computed magnetic moment on Pt is 1.1 μ_B, much larger than on Cu (0.29 μ_B) in $CaCuO_2$. Comparing $NaPtF_2$ with $CaCuO_2$, while the magnetic moment is larger for Pt(I), the local spin population is very similar to that of Cu(II) with a hole in the $d_{x^2-y^2}$. Both are formally d^9 systems. We have no simple explanation yet for the difference in their magnetization.

The instability of $NaPtF_2$ in the *P*4/*mmm* structure led us to explore MD annealing calculations on $NaPtF_2$. A new structure (space group: *Amm*2), shown in Figure 17, was reached. This $NaPtF_2$ phase, whose phonon spectrum showed no imaginary frequencies, is calculated to be 0.20 eV per $NaPtF_2$ more stable thermodynamically than the original *P*4/*mmm* structure.

In the *Amm*2 structure, the Pt atoms are in a distorted square-planar coordination, which can be viewed as the intersection of two 1-D chains. One chain has a Pt−F bond at 2.315 Å, F−Pt−F = 170°, in the other chain Pt−F is calculated as 2.250 Å, F−Pt−F = 175°. The computed magnetic moment on Pt in the FM state is 1.3 μ_B, larger than in the Kentuckia framework (1.1 μ_B).

There is a clear structural relationship between the new $NaPtF_2$ structure (Figure 17) and the *P*4/*mmm* structure we began with. As Figure 17 and the text above describe, we have in the *Amm*2 structure slightly corrugated and distorted PtF_2 planar sheets. But they are not placed directly above each other along c, as in the *P*4/*mmm* structure. Instead, the layers slip relative to each other, so that a Pt of one layer is above a F of the next layer.

We moved next to evolutionary structure prediction, utilizing the USPEX program. Figure 18 (right) shows the lowest energy structure with the space group, $R\bar{3}m$. Each Pt atom is bonded to two F atoms (Pt−F = 2.00 Å, which is slightly longer than average Pt−F distance at 1.90 Å) and six Pt atoms (Pt−Pt = 3.07 Å). *What we have effectively is a hexagonal sheet of* $(PtF_2)^-$ *units weakly bonded between the Pt's*. The phonon dispersion of the

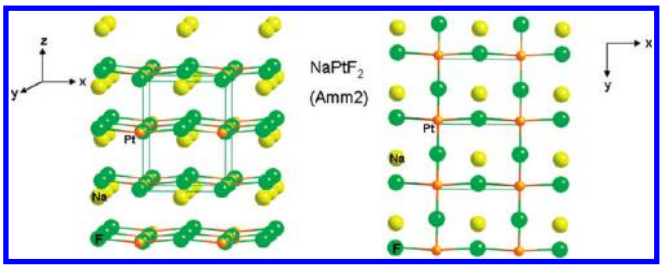

Figure 17. *Amm*2 structure of $NaPtF_2$ optimized with DFT.

$R\bar{3}m$ $NaPtF_2$ indicates that it is dynamically stable. The structure is 0.76 eV per $NaPtF_2$ more favorable thermodynamically than the original *P*4/*mmm* structure, and more stable by 0.56 eV than *Amm*2 $NaPtF_2$ obtained by annealing. It may be that there are high energy barriers among these metastable structures, for they differ much. The computed magnetic moment on Pt in the FM state is 0.0 μ_B, which is quite different with Kentuckia (1.1 μ_B). and *Amm*2 structure (1.3 μ_B). The DOS are shown in the Supporting Information.

Given the crystallochemical similarity of fluoride (F^-) and hydride (H^-), we also investigated $NaPtH_2$ and obtained a similar structure, a hexagonal net of PtH_2^- molecules. The band structure of nonmagnetic $NaPtF_2$ is shown in Figure 18 (right). $NaPtH_2$ is similar (see Supporting Information). Note the striking steep band crossing the Fermi Level. The slopes and positions of maxima in this band are in part a consequence of the primitive unit cell choice. This half-filled band is mainly Pt d_{z^2}, with some F (or H) admixture. This is consistent with the crystal field splitting in a d^9 linear PtF_2^-, in which one would expect a high-lying half-filled d_{z^2}. Linear PdH_2^{2-} units (one electron more) are known in the structure of Li_2PdH_2 and Na_2PdH_2 of Noréus et al.[43,44]

Interestingly a USPEX study of $NaPtH_2$ in a larger unit cell led us to still another defect perovskite structure, shown in Figure 19.

3. Conclusions

We have examined theoretically the structures and electronic properties of a variety of ABX_2 structures in the *P*4/*mmm* Kentuckia family, including the known $CaCuO_2$ and $SrFeO_2$ compounds. The use of a supercell allowed us to compute correctly the magnetic properties of $CaCuO_2$ (it is AFM) but failed to give any band gap for this phase. For $SrFeO_2$, our calculations (and assigned d orbital splitting) in general agree with previous theoretical work; we find the material to be a direct-gap semiconductor.

We also looked at a number of more atypical variations of this structure, all as yet unknown. These include $SrFeC_2$, $SrFe(C_2)_2$, $SrFe(H_2)_2$, $AeTiO_2$, and $APtF_2$. Among these the $SrFe(C_2)_2$, $AeTiO_2$, and $NaPtF_2$ phases were especially interesting. In a number of cases our structural search lead us quite far away from the parent Kentuckia structure.

The hypothetical carbide, $SrFe(C_2)_2$, contained C_2 units with a C−C distance of 1.267 Å. We were most surprised by the $SrTiO_2$ structure and its seemingly 1-D metallic behavior. A single band crosses the Fermi level in the c direction (along Γ→Z). There is Ti−Ti σ and π bonding in this structure, even

(43) Noréus, D.; Tomkinson, J. *Chem. Phys. Lett.* **1988**, *154*, 5.
(44) Kadir, K.; Noréus, D. *Z. Phys. Chem. Neue. Fol.* **1989**, *163*, 231.

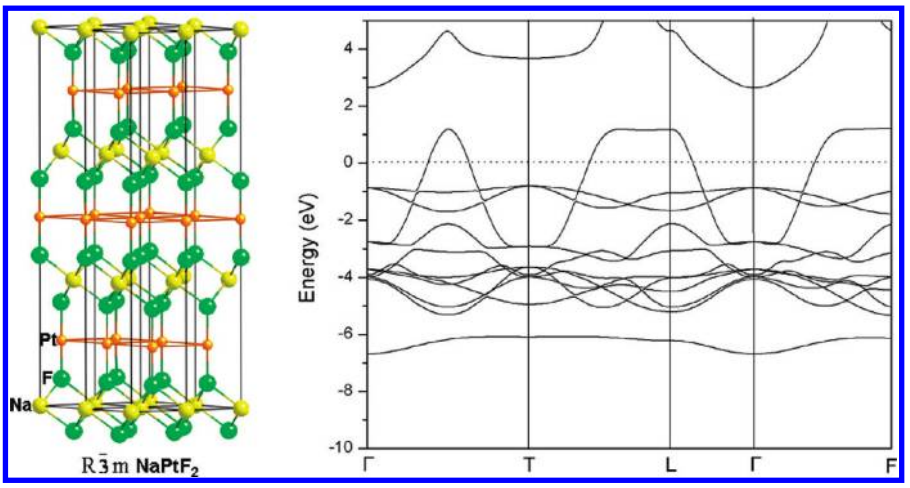

Figure 18. Lowest energy $NaPtF_2$ ($R\bar{3}m$) structure found by USPEX, and its band structure.

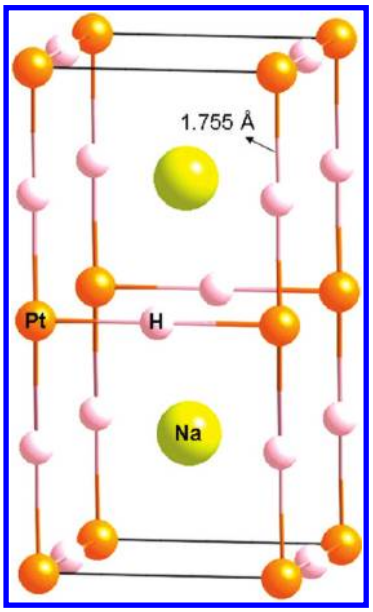

Figure 19. Lowest energy $NaPtH_2$ ($Pmmm$) by USPEX.

at a Ti−Ti separation of 3.6 Å. That separation may be tuned by the alkaline earth ion; it is smaller for Mg, Be, and $CaTiO_2$ and bigger for $BaTiO_2$.

For $NaPtF_2$ the Kentuckia structure showed some residual Pt−Pt bonding, but more interestingly, we found two more stable structures. One of these has a fascinating hexagonal sheet of weakly interacting $(PtF_2)^-$ units.

A common feature among all compounds investigated is a partially filled d block. This leads to spin-polarization; most of the compounds we have examined ($CaCuO_2$, $SrFeO_2$, $SrFeC_2$, $SrFeS_2$, $SrFe(H_2)_2$, $NaPtF_2$, $LiPtF_2$, $KPtF_2$, $CsPtF_2$, $SrPtO_2$, and $LaPtO_2$) have antiferromagnetically coupled ground states. Only ($SrFe(C_2)_2$) was FM. An attempt was made to assign the d orbital splitting in the compounds studied. This proved problematic; the large splitting of spin states for many of the magnetic metal centers made it difficult to assign a single level ordering diagram that would be appropriate for both spins. Nevertheless, in this structural type most of the time we have a level pattern that puts the $d_{x^2-y^2}$ level highest. The d_{z^2} levels are sometimes below, sometimes above the $d_{xz}+d_{yz}$; the d_{xy} states are in-between in energy.

The Kentuckia structure is not only the geometry of the known and interesting $CaCuO_2$ and $SrFeO_2$ phases, but leads to a number of other realizations with intriguing electronic properties.

4. Methods Summary

DFT Method. The calculations are based on the plane wave/pseudopotential approach using the computer program VASP[45,46] employing the LSDA+U [The "LSDA+U" method for Fe with $U = 4.5$ eV and $J = 0$ on Fe[17] predicted the correct ground state, $U = 0$ did not. For Cu, $U = 7.5$ eV and $J = 0$.] corrections[47] of the PBE type, and the projected-augmented wave (PAW)[48,49] method. All calculations included spin polarization, except as noted; also a $\sqrt{2} \times \sqrt{2} \times 2$ supercell, a 500 eV energy cutoff for plane waves and a ($15 \times 15 \times 15$) set of Monkhorst Pack grid of k-points. The supercell with four Cu or Fe atoms is the minimum cell that will allow for a computational distinction to be made between a ferromagnetic and an antiferromagnetic crystal. We allow all structural parameters (atomic position, lattice constants, and symmetry) to relax. Phonon calculations are carried out using VASP combined with PHON[50] in a $2 \times 2 \times 2$ supercell. The evolutionary algorithm USPEX[51−53] was employed to find the lowest energy structures; the method has been successfully tested and applied to many other systems. The calculations were carried out at ~0 GPa, consistent with our DFT calculations.

Extended Hückel Theory. After the structures are optimized with DFT, extended Hückel (eH)[54] calculations are performed, utilizing the YAeHMOP program.[55] The default extended Hückel parameters are employed. The eH calculations

(45) Perdew, J. P.; Burke, K.; Ernzerhof, M. *Phys. Rev. Lett.* **1997**, *78*, 1396.
(46) Kresse, G.; Hafner, J. *Phys. Rev. B* **1993**, *47*, 558.
(47) Dudarev, S. L.; Botton, G. A.; Savrasoz, S. Y.; Humphreys, C. J.; Sutton, A. P. *Phys. Rev. B* **1998**, *57*, 1505.
(48) Bloechl, P. E. *Phys. Rev. B* **1994**, *50*, 17953.
(49) Kresse, G.; Joubert, D. *Phys. Rev. B* **1999**, *59*, 1758.
(50) Vocadlo, L.; Alfè, D.; Brodholt, J.; Gillan, M. J.; Price, G. D. *Geophys. Res. Lett.* **1999**, *26*, 1231.
(51) Glass, C. W.; Oganov, A. R.; Hansen, N. *Comput. Phys. Commun.* **2006**, *175*, 713.
(52) Oganov, A. R.; Glass, C. W. *J. Chem. Phys.* **2006**, *124*, 244704.
(53) Oganov, A. R.; Glass, C. W; Ono, S. *Earth Planet Sci. Lett.* **2006**, *241*, 95.
(54) Hoffmann, R. *J. Chem. Phys.* **1963**, *39*, 1397.
(55) Landrum, G. A. ***viewkel*** (ver 3.0). ***viewkel*** is distributed as part of the ***YAeHMOP*** extended Hückel molecular orbital package and is freely available on the WWW at http://overlap.chem.cornell.edu:8080/YAeHMOP.html

are certainly less reliable for structures, but offer a number of analytical tools for exploring the nature of bonding. With the DFT program we use, it is difficult to get reliable atomic and orbital contributions to the density of states (DOS).[56]

Acknowledgment. Calculations were performed in part at the Cornell NanoScale Facility, a member of the National Nanotechnology Infrastructure Network, which is supported by the National Science Foundation. Our work at Cornell was supported by the National Science Foundation through Grants CHE-0613306 and CHE-0910623. This research was also supported by the National Science Foundation through TeraGrid resources provided by NCSA.

Supporting Information Available: The calculated parameters, the band structures and DOS, phonon dispersion, and the impact of different Hubbard U values. This material is available free of charge via the Internet at http://pubs.acs.org.

(56) The RWIGS values are the default parameters from the pseudopotential file. There are real problems with VASP projected DOS values not adding up to the total DOS.